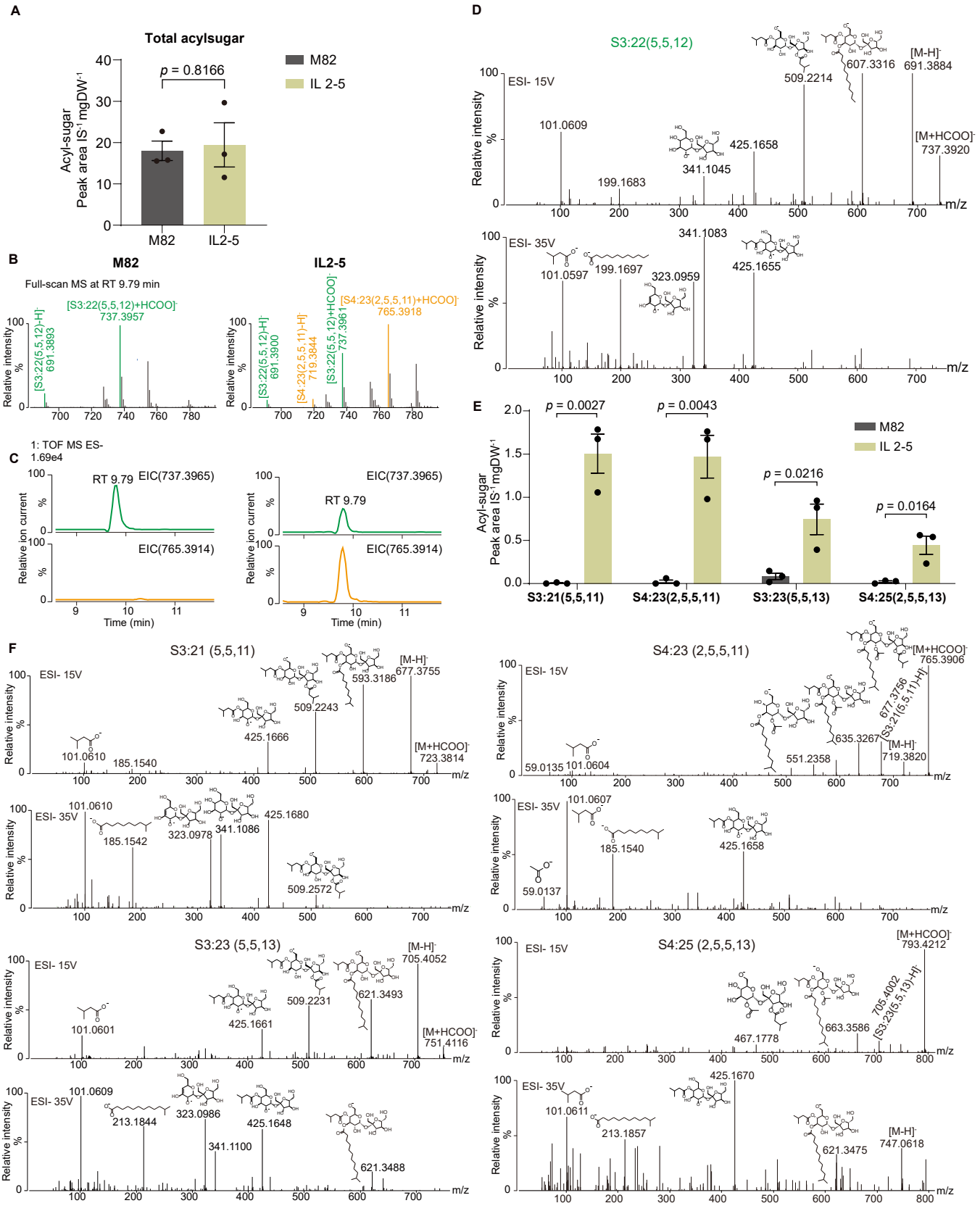

Figure S1. Leaf surface acylsugar profiling of IL2-5 and M82. (A) Quantification of total acylsugars in M82 and IL2-5. Peak area ratios (acylsugar/internal standard) normalized by leaf dry weight (DW) are shown. Data presented as means ± SEM (n = 3 biologically independent samples). Statistical significance determined by unpaired two-tailed *t*-test. **(B)** Full-scan MS at RT 9.79 min of co-eluting peak. The full-scan spectrum indicated the ions at m/z 737.3965 and 765.3914 co-eluted at RT 9.79 in IL2-5, whereas the ions at m/z 765.3914 was absent in M82. **(C)** EIC for the ions of two acylsugars from M82 (left panel) and IL2-5 (right panel). Selected ion masses of the corresponding acylsugars are shown in the parentheses following the EIC, with maximum ion counts indicated in the upper left of the figure. **(D)** Negative ionization mode, target MS/MS of the acylsugar S3:22(5,5,12) (m/z 737.3965) from IL2-5 at different collision energies. Spectra are shown at 15 V and 35 V collision energies to induce fragmentation. **(E)** Quantification of the four long-branched-chain acylsugars in M82 and IL2-5. Peak area ratios (acylsugar/internal standard) normalized by leaf DW are shown. Data presented as means ± SEM (n = 3 biologically independent samples). Statistical significance determined by unpaired two-tailed *t*-test. **(F)** Negative ionization mode, target MS/MS of four specific acylsugars from IL2-5 at different collision energies. Spectra are shown at 15 V and 35 V collision energies to induce fragmentation.

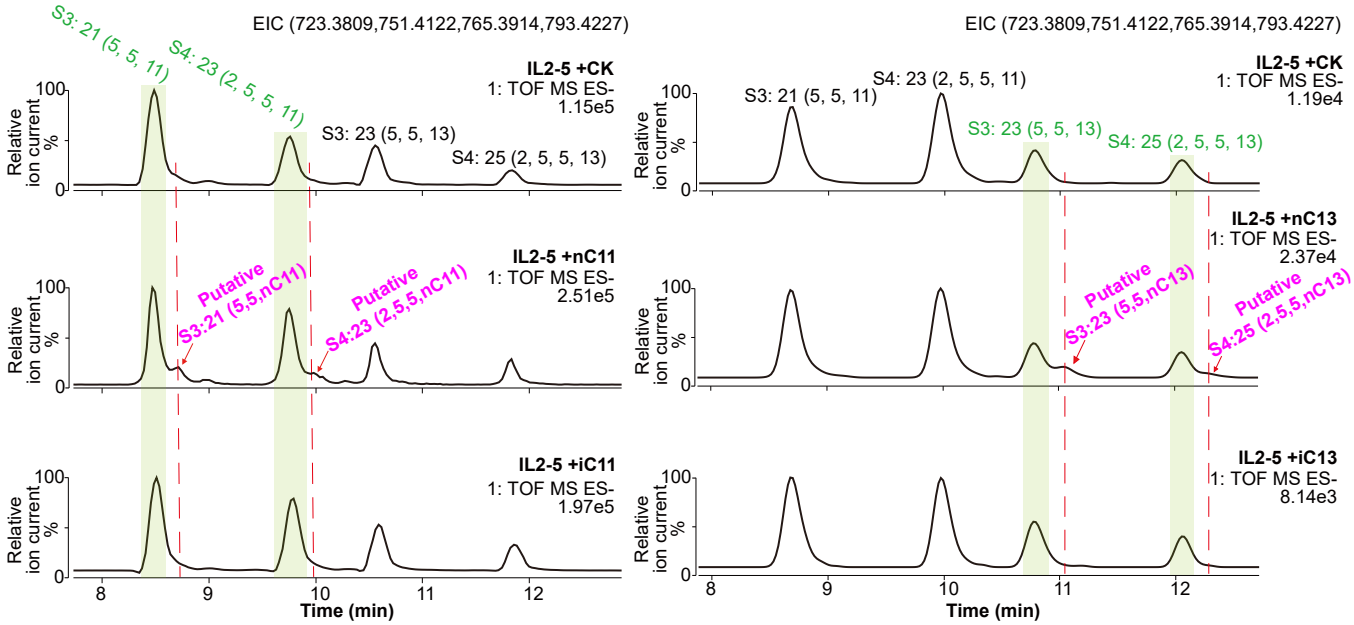

Figure S2. Exogenous fatty acid application provides evidence that the long acyl chains of the four specific acylsugars in IL2-5 are not straight-chain. Representative LC/MS extracted ion chromatograms (EICs) of four specific acylsugars in IL2-5 following exogenous application of C11 fatty acids iC11/nC11 (left panel) and C13 fatty acids iC13/nC13 (right panel). The endogenous IL2-5 peaks are assigned as iC11- or iC13-containing acylsugars based on GC-MS analysis of released acyl chains with authentic standards (Fig. 1B). Red arrowheads indicate new peaks detected specifically after application of nC11 or nC13. These peaks showed the same m/z values as the corresponding endogenous C11- or C13-containing acylsugars, with mass errors within 10 ppm, but eluted slightly later on the reverse-phase C18 column, consistent with putative straight-chain C11 or C13 acylsugar products. No comparable new peaks were detected in control plants or after application of iC11 or iC13. Chromatograms are normalized to the largest peak within each sample. Selected ion masses are shown in parentheses after each EIC, and maximum ion counts are indicated in the upper right corner.

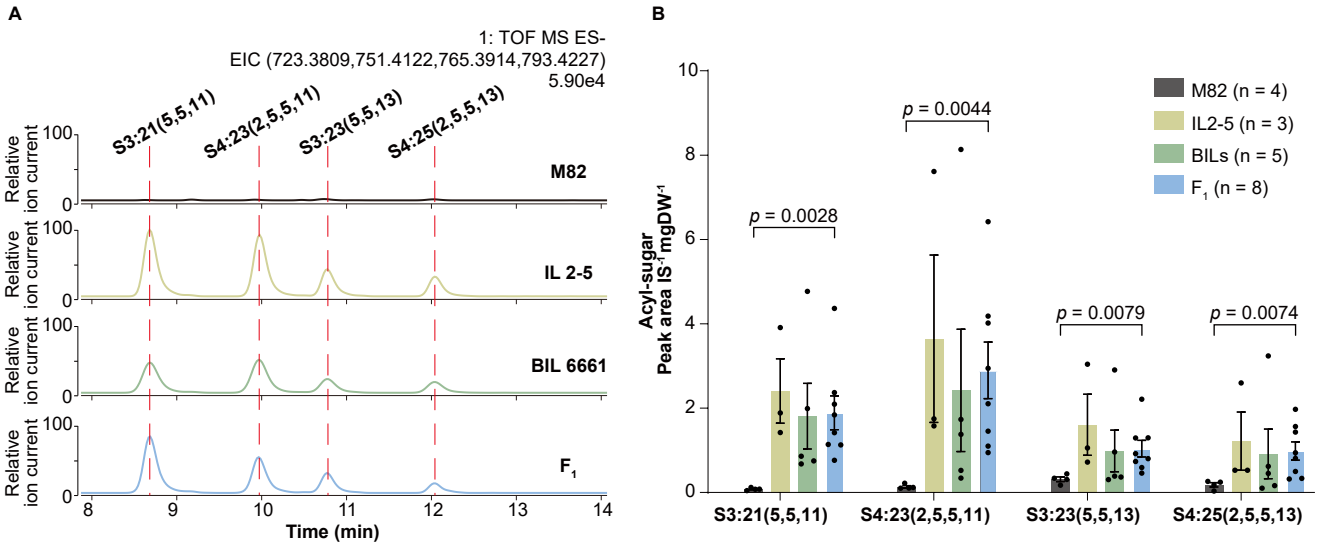

Figure S3. Genetic dominance of the branched-chain acylsugar trait demonstrated in F_1 hybrids from BIL6661 × M82 cross. (A) LC/MS EICs of four specific acylsugars from M82, IL2-5, BIL 6661, and the hybrid F_1 plant. Chromatograms normalized to the largest peak across all samples. Selected ion masses shown in parentheses following the EIC, with maximum ion counts indicated in the upper right of the figure. **(B)** Quantitative comparison of the four specific long-branched-chain acylsugars across M82, BILs, IL2-5, and the F_1 plant. Values represent peak area ratios of acylsugar to internal standard (IS), normalized by leaf dry weight (DW). Data presented as means ± SEM, n represents biologically independent replicates. Statistical significance determined by unpaired two-tailed *t*-test with Welch's correction.

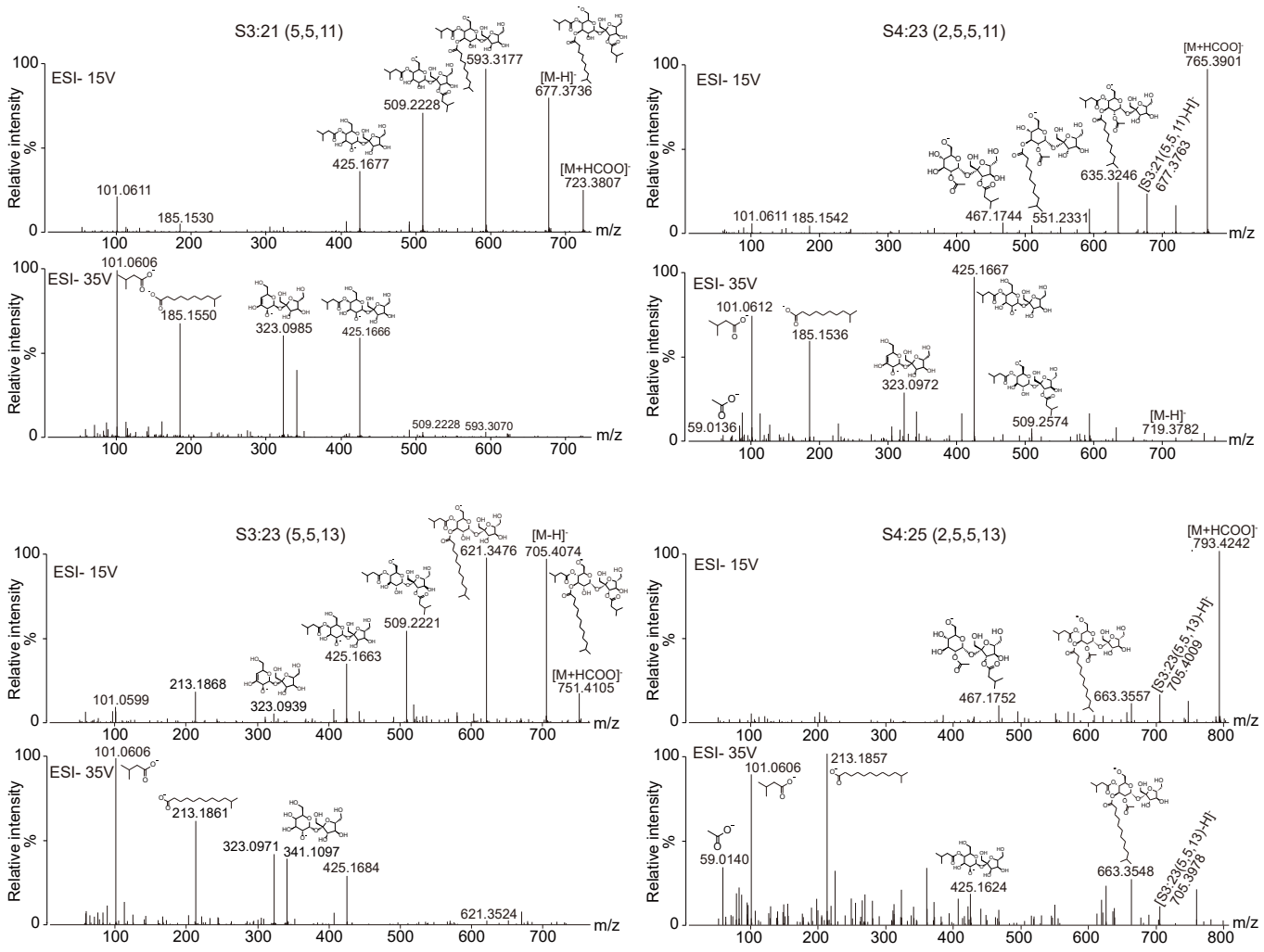

Figure S4. LC MS/MS fragmentation of the four long-branched-chain acylsugars from M82 transgenic plants transformed with *SpBACS1* under its native promoter. Negative ionization mode mass spectra of the four specific acylsugars from the transgenic plant (*proSpBACS1::SpBACS1* in M82) at different collision energies. Spectra are shown at 15 V and 35 V collision energies to induce fragmentation.

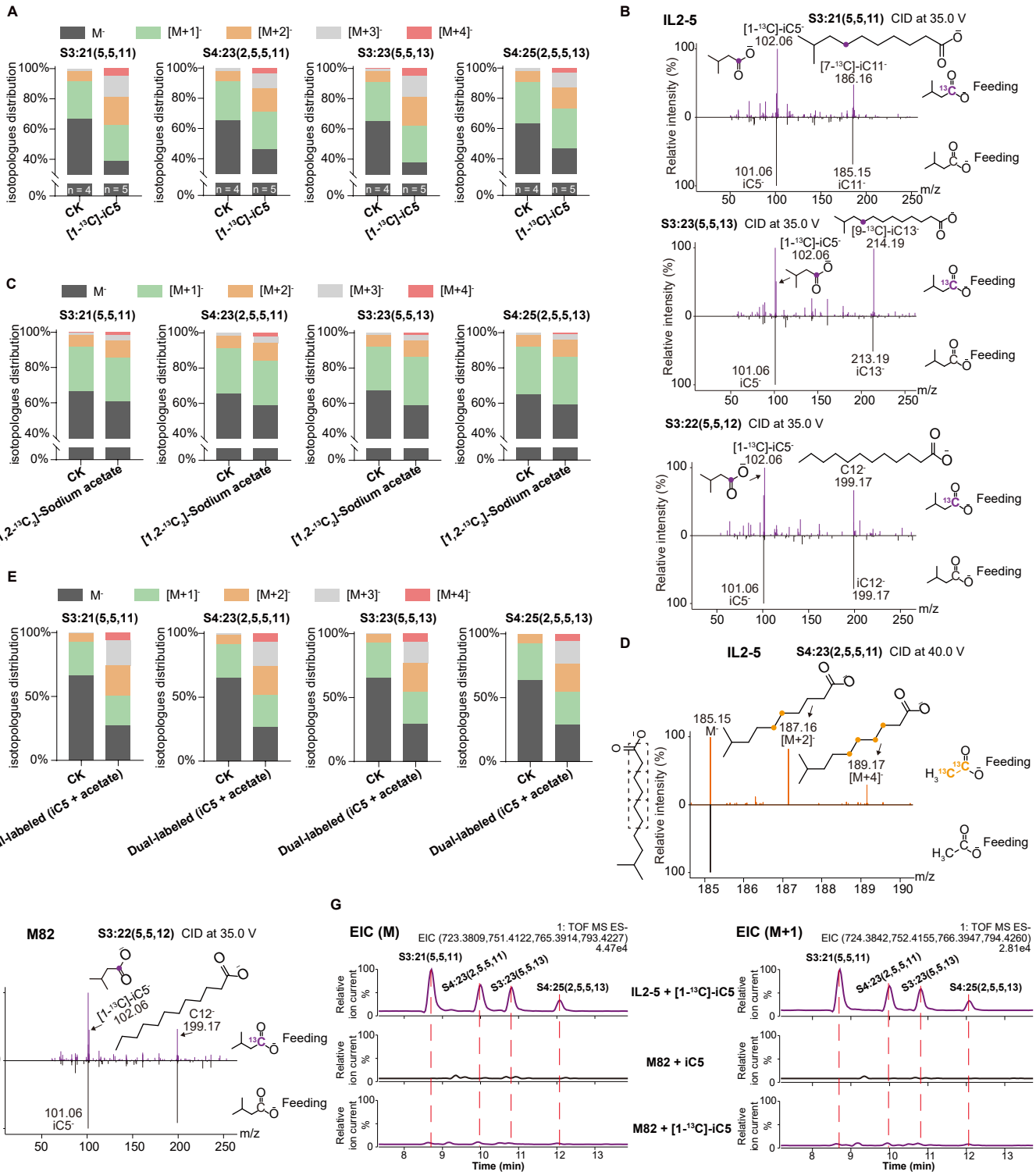

Figure S5. Isotopologue analysis of long-branched-chain acylsugars following isotope labeling. (A) Isotopologues distribution ([M]$^-$, [M+1]$^-$, [M+2]$^-$, [M+3]$^-$, and [M+4]$^-$) of four acylsugars in IL2-5 plant fed with isotope-labeled [1-^{13}C]-iC5 compared to control plants fed with non-labeled iC5. The analyzed acylsugars include S3:21(5,5,11), S4:23(2,5,5,11), S3:23(5,5,13), and S4:25(2,5,5,13). Data are presented as mean proportions normalized to a total of 100% for each acylsugar. n represents biologically independent replicates. CK, control sample. **(B)** LC-MS/MS fragmentation analysis of acylsugars S3:21(5,5,11), S3:23(5,5,13) and S3:22(5,5,12), showing MS spectra of one-carbon labeled ([M+1]$^-$) versus non-labeled (M$^-$) iC5 and C12 ions. Spectra from IL2-5 plants fed with [1-^{13}C]-iC5 and control plants fed with non-labeled iC5 are vertically stacked. **(C)** Isotopologues distribution ([M]$^-$, [M+1]$^-$, [M+2]$^-$, [M+3]$^-$, and [M+4]$^-$) of four acylsugars in IL2-5 plant fed with isotope-labeled 1,2-$^{13}C_2$-sodium acetate compared to control plants fed with non-labeled sodium acetate. The analyzed acylsugars include S3:21(5,5,11), S4:23(2,5,5,11), S3:23(5,5,13), and S4:25(2,5,5,13). Data are presented as mean proportions normalized to a total of 100% for each acylsugar (n = 6 biologically independent samples). CK, control sample. **(D)** LC-MS/MS fragmentation analysis of acylsugars S4:23(2,5,5,11), showing MS spectra of two- and four-carbon labeled ([M+2]$^-$ and [M+4]$^-$) versus non-labeled (M$^-$) iC11 fragment ions. Spectra from IL2-5 plants fed with 1,2-$^{13}C_2$-sodium acetate and control plants fed with non-labeled sodium acetate are stacked vertically. Possible positions of isotopic incorporation in iC11 or iC13 are highlighted by black dashed boxes. **(E)** Isotopologues distribution ([M]$^-$, [M+1]$^-$, [M+2]$^-$, [M+3]$^-$, and [M+4]$^-$) of four acylsugars in IL2-5 plant co-fed with [1-^{13}C]-iC5 and 1,2-$^{13}C_2$-sodium acetate compared to control plants co-fed with non-labeled iC5 and sodium acetate. The analyzed acylsugars include S3:21(5,5,11), S4:23(2,5,5,11), S3:23(5,5,13), and S4:25(2,5,5,13). Data are presented as mean proportions normalized to a total of 100% for each acylsugar (n = 5 biologically independent samples). CK, control sample. **(F)** LC-MS/MS fragmentation analysis of acylsugars S3:22(5,5,12), showing MS spectra of one-carbon labeled ([M+1]$^-$) versus non-labeled (M$^-$) iC5 and C12 ions. Spectra from M82 plants fed with [1-^{13}C]-iC5 and control plants fed with non-labeled iC5 are vertically stacked. **(G)** Representative LC-MS extracted ion chromatograms (EICs) of four selected acylsugars in IL2-5 and M82 plants fed with [1-^{13}C]-iC5 or unlabeled iC5. For each acylsugar, the left panels show unlabeled acylsugars (M$^-$), and the right panels show one-carbon-labeled acylsugars ([M+1]$^-$). Chromatograms are normalized to the largest peak across all samples. Selected ion masses shown in parentheses following the EIC, with maximum ion counts indicated in the upper right.

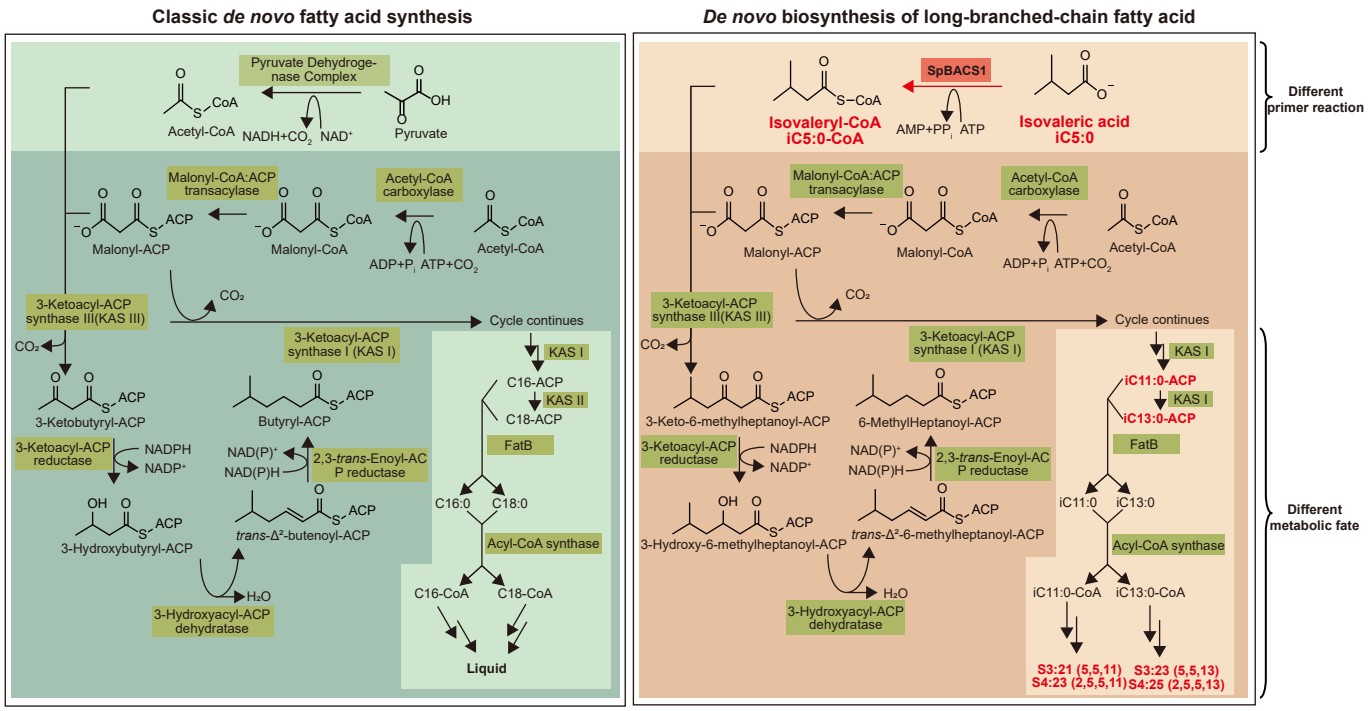

Figure S6. Detailed metabolic pathway comparison between the proposed SpBACS1-mediated long-branched-chain fatty acid synthesis and classical *de novo* fatty acid biosynthesis. Expanded schematic of the metabolic pathways depicted in Fig. 3G, illustrating the acyl-CoA primer formation step and chain elongation step for both SpBACS1-mediated long-branched-chain acylsugar biosynthesis and classical *de novo* fatty acid biosynthesis.The proposed pathway of fatty acid biosynthesis is based on previous publications [43,44].

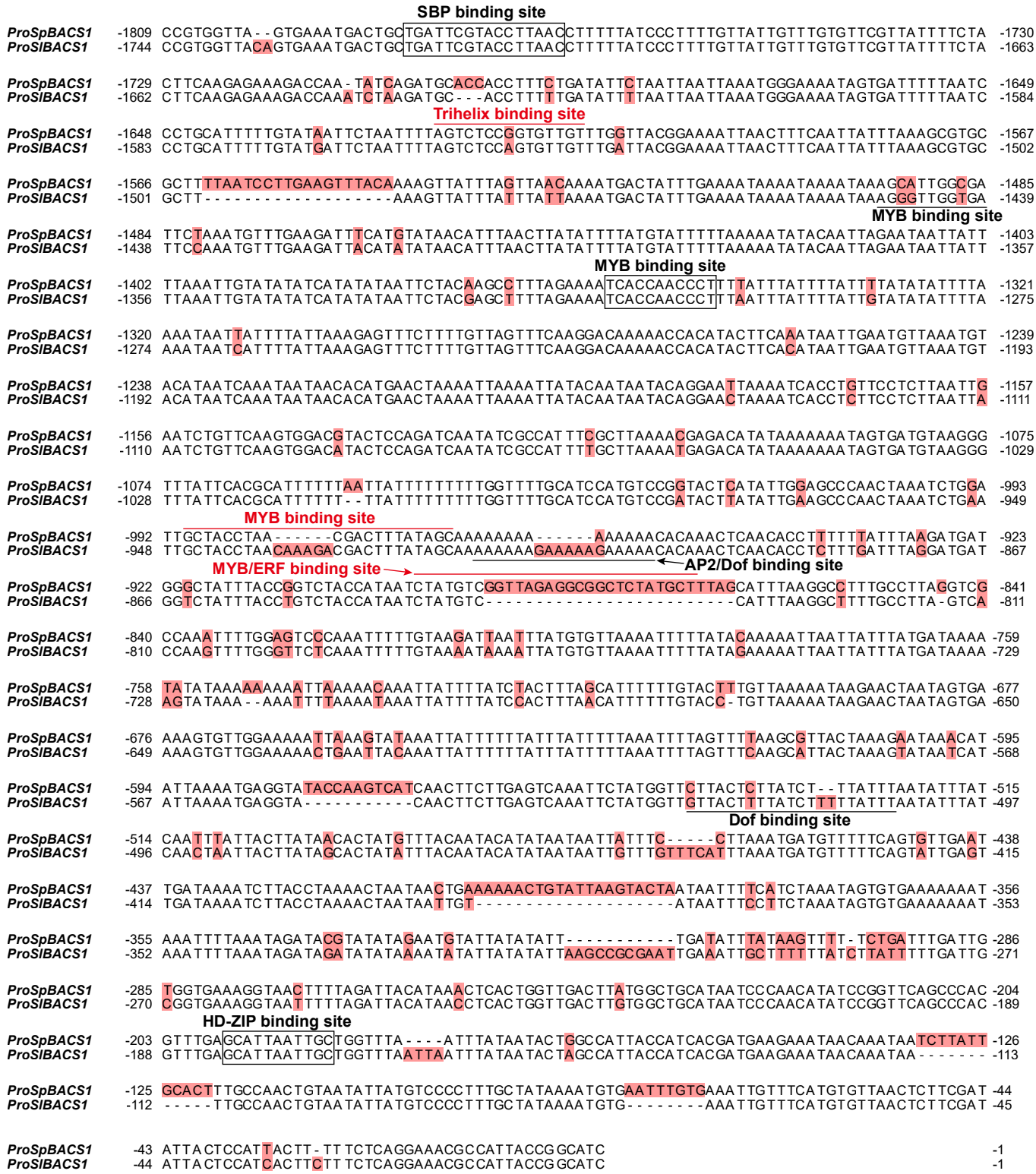

Figure S7. Promoter sequence alignment and cis-element analysis comparing *SpBACS1* and *SlBACS1*. Sequence alignment of *SpBACS1* and *SlBACS1* promoter regions with putative cis-elements for transcription factor binding sites predicted using PlantRegMap. Black boxes indicate predicted cis-elements common to both promoters. Red and black lines denote predicted cis-elements unique to *SpBACS1* and *SlBACS1* promoters, respectively.

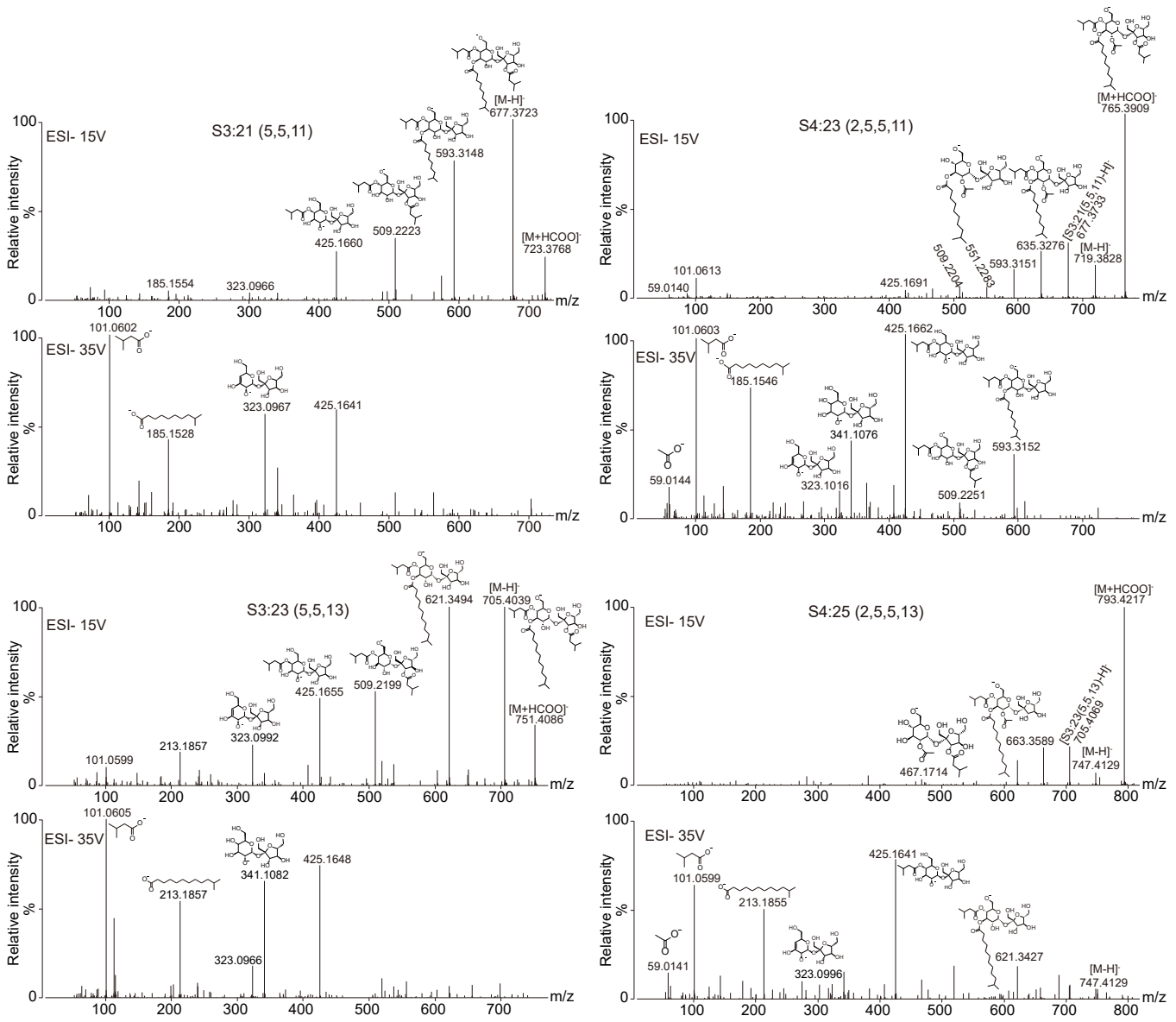

Figure S8. LC MS/MS fragmentation of the four long-branched-chain acylsugars from M82 transgenic plants transformed with *SlBACS1* under the *SpBACS1* promoter. Negative ionization mode mass spectra of the four specific acylsugars from the transgenic plant (*proSpBACS1::SlBACS1* in M82) at different collision energies. Spectra are shown at 15 V and 35 V collision energies to induce fragmentation.

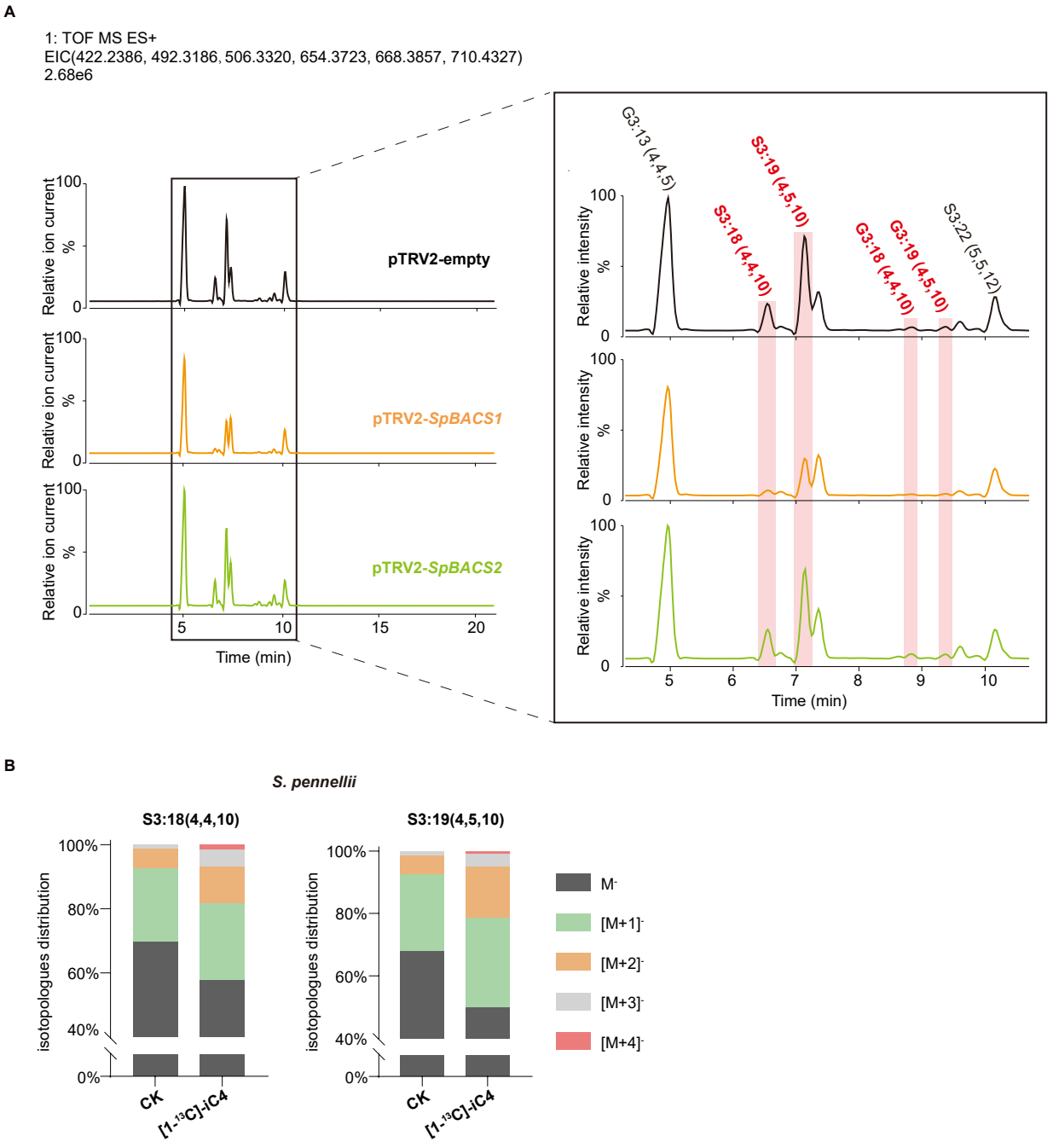

Figure S9. LC/MS analysis of iC10-containing and other acylsugars in *S. pennellii* VIGS lines silencing *SpBACS1* and *SpBACS2*. (A) Representative LC/MS EICs of selected acylsugars in *S. pennellii* VIGS lines silencing *SpBACS1* (pTRV2-*SpBACS1*), *SpBACS2* (pTRV2-*SpBACS2*), and control plants (pTRV2-empty). Chromatograms normalized to the largest peak across all three samples. Selected ion masses shown in parentheses following the EIC, with maximum ion counts indicated in the upper left of the figure. Light red bands in zoomed-in chromatograms highlight reduced acylsugar levels in pTRV2-*SpBACS1* plants. **(B)** Isotopologues distribution ($[M]^-$, $[M+1]^-$, $[M+2]^-$, $[M+3]^-$, and $[M+4]^-$) of two acylsugars in *S. pennellii* plant fed with isotope-labeled [1-^{13}C]-iC4 compared to control plants fed with non-labeled iC4. These analyzed acylsugars include S3:18(4,4,10) and S3:19(4,5,10). Data are presented as mean proportions normalized to a total of 100% for each acylsugar (n = 4 biologically independent samples). CK, control sample.

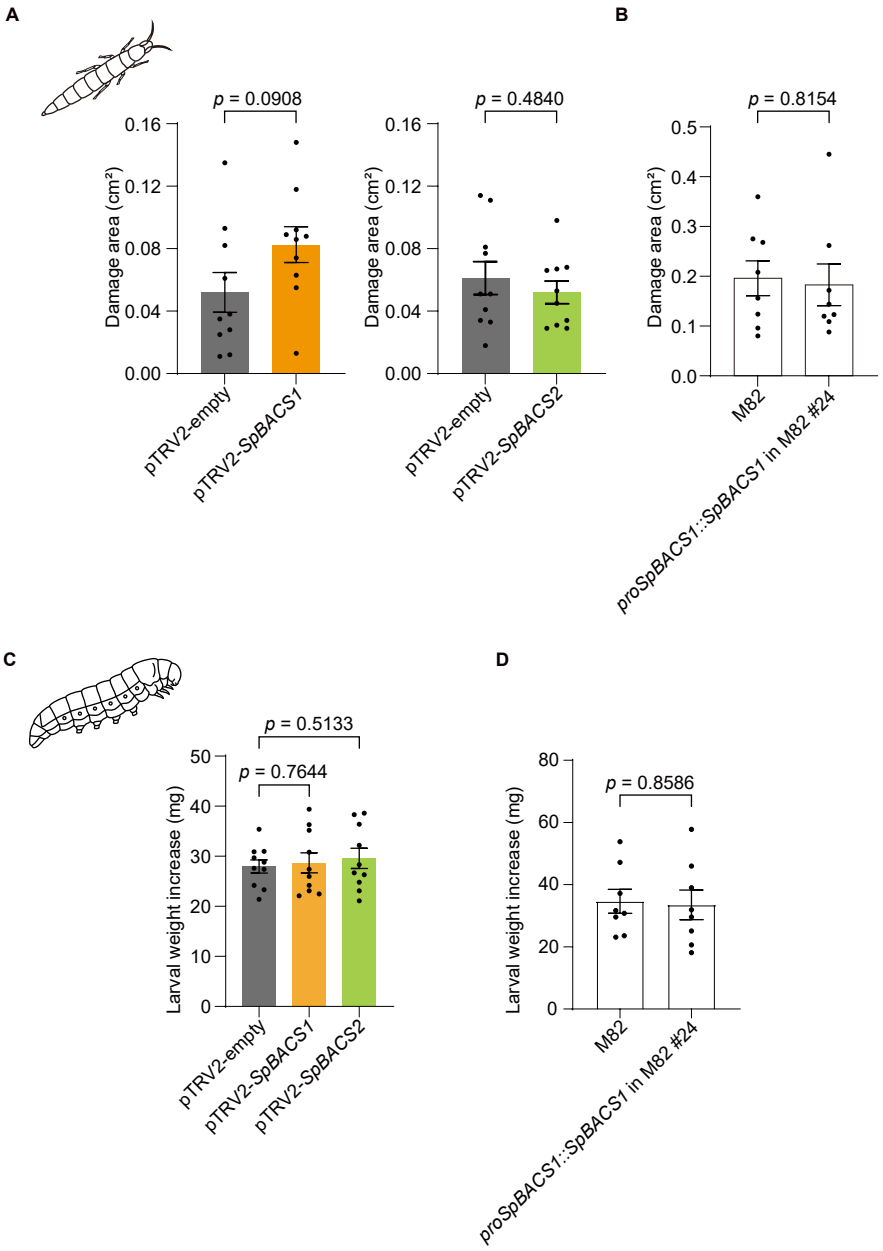

Figure S10. Effects of SpBACS1-mediated long-branched-chain acylsugars on herbivore resistance. (A) Quantification of leaf damage caused by western flower thrips (*Frankliniella occidentalis*) feeding on *S. pennellii* VIGS plants with silenced *SpBACS1* or *SpBACS2*. Data presented as means ± SEM (n = 10 biologically independent samples). Statistical significance determined by unpaired two-tailed *t*-test. **(B)** Quantification of leaf damage caused by western flower thrips (*F. occidentalis*) feeding on M82 transgenic plants expressing *SpBACS1* driven by its native promoter. Data presented as means ± SEM (n = 8 biologically independent samples). Statistical significance determined by unpaired two-tailed *t*-test. **(C)** Quantification of cotton bollworm (*Helicoverpa armigera*) larval weight gain after feeding on *S. pennellii* VIGS plants with silenced *SpBACS1* or *SpBACS2*. Data presented as means ± SEM (n = 10 biologically independent samples). Statistical significance determined by unpaired two-tailed *t*-test. **(D)** Quantification of cotton bollworm (*H. armigera*) larval weight gain after feeding on M82 transgenic plants expressing *SpBACS1* driven by its native promoter. Data presented as means ± SEM (n = 8 biologically independent samples). Statistical significance determined by unpaired two-tailed *t*-test.

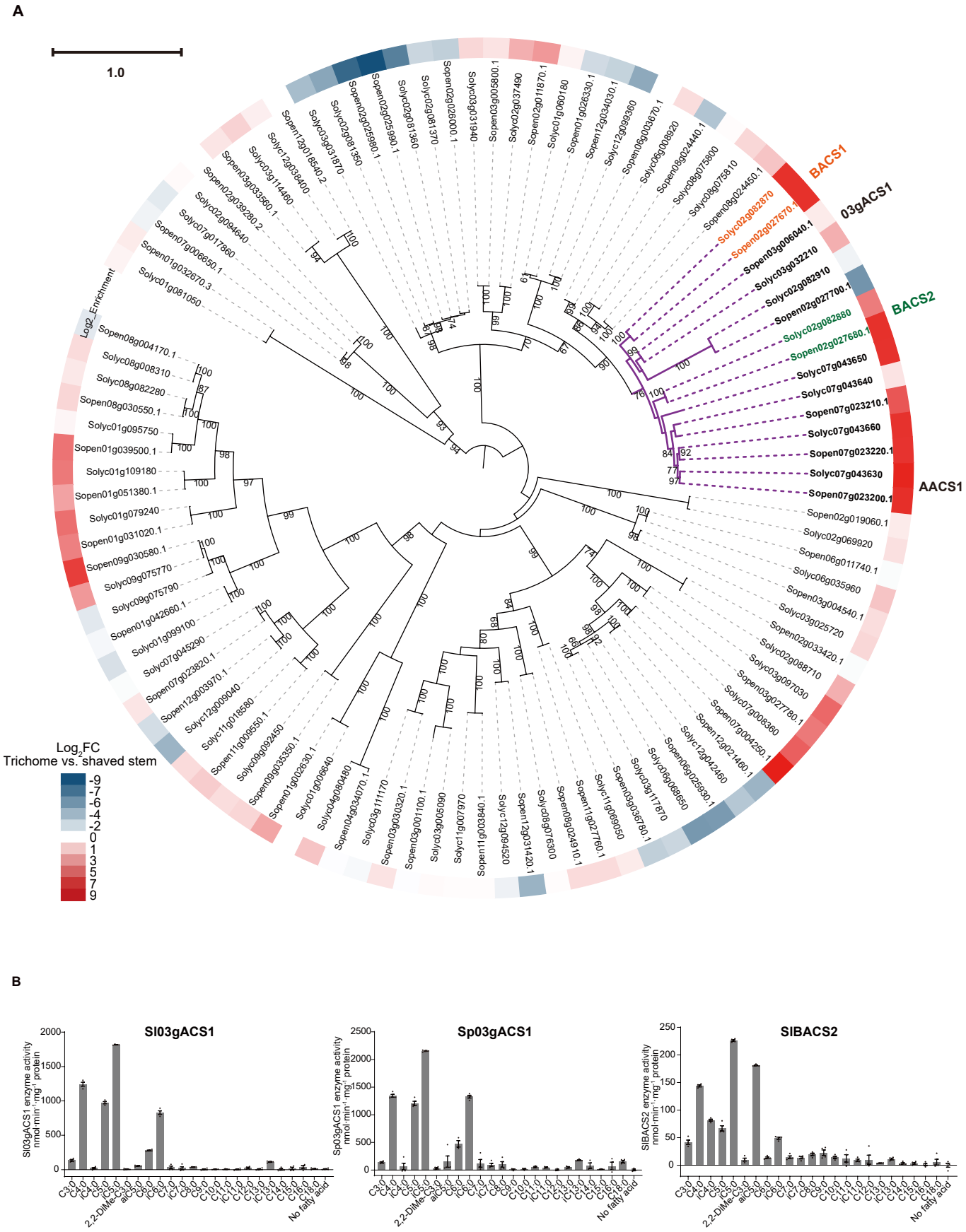

Figure S11. Phylogenetic analysis and biochemical characterization of ACS family enzymes in *S. lycopersicum* and *S. pennellii*. (A) Phylogenetic tree showing relationships among ACS family members in *S. lycopersicum* and *S. pennellii*, with trichome-enriched expression patterns. Red-blue color gradient represents trichome enrichment as log2 fold change (log2FC) for trichome vs. shaved stem expression. **(B)** Substrate specificity of Sl03gACS1, Sp03gACS1 and SlBACS2 across a broad spectrum of fatty acids varying in chain length and branching pattern with Coenzyme A (CoA) as co-substrate. Enzyme activities shown as means ± SEM (n = 4 independent experiments).